Pergamon

*Journal of Structural Geology*, Vol. 18, No. 9, pp. 1167 to 1172, 1996

PII: S0191-8141(96)00039-9
0191-8141/96 $15.00 + 0.00

## Brevia

# SHORT NOTES

# Non-ellipsoidal inclusions as geological strain markers and competence indicators

S. H. TREAGUS

Department of Earth Sciences, University of Manchester, Manchester M13 9PL, U.K.

and

P. J. HUDLESTON and L. LAN

Department of Geology and Geophysics, University of Minnesota, Minneapolis, MN 55455, U.S.A.

(*Received* 11 *August* 1995; *accepted in revised form* 4 *March* 1996)

**Abstract**—Geological objects that do not deform homogeneously with their matrix can be considered as inclusions with viscosity contrast. Such inclusions are generally treated as initially spherical or ellipsoidal. Theory shows that ellipsoidal inclusions deform homogeneously, so they maintain an ellipsoidal shape, regardless of the viscosity difference. However, non-ellipsoidal inclusions deform inhomogeneously, so will become irregular in shape. Geological objects such as porphyroblasts, porphyroclasts and sedimentary clasts are likely to be of this kind, with initially rectilinear, prismatic or superelliptical section shapes.

We present two-dimensional finite-element models of deformed square inclusions, in pure shear (parallel or diagonal to the square), as a preliminary investigation of the deformation of non-ellipsoidal inclusions with viscosity contrast. Competent inclusions develop marked barrel shapes with horn-like corners, as described for natural ductile boudins, or slightly wavy rhombs. Incompetent inclusions develop 'dumb-bell' or bone shapes, with a surprising degree of bulging of the shortened edges, or rhomb to sheath shapes. The results lead to speculation for inclusions in the circle to square shape range, and for asymmetric orientations. Anticipated shapes range from asymmetric barrels, lemons or flags for competent inclusions, to ribbon or fish shapes for incompetent inclusions. We conclude that shapes of inclusions and clasts provide an important new type of strain marker and competence criterion. 

## INTRODUCTION

The success of measuring strain in rocks depends on finding useful strain markers. This contribution addresses the question of strain markers that do not deform homogeneously with their matrix, such as varied clasts in a deformed conglomerate. Traditional theory treats such strain markers as spherical or ellipsoidal inclusions, but it may not be appropriate to approximate them as such. We present a preliminary study of the deformation of non-ellipsoidal inclusions, using finite-element models of deformed square inclusions, with different viscosity from the matrix. These results, together with predictions for other classes of inclusion shape, provide new criteria for estimating strain and viscosity contrasts in rocks.

## THEORY FOR DEFORMED ELLIPSOIDAL INCLUSIONS

A considerable body of work exists, in the geological and material sciences literature, for the theory of deformation of an inclusion different from its matrix (Eshelby 1957, Gay 1968a,b, 1976, Bilby *et al.* 1975, Bilby & Kolbuszewski 1977, Lisle *et al.* 1983, Lisle 1985, Freeman 1987). These studies demonstrate, for Newtonian materials, that an isolated ellipsoidal inclusion in cohesive contact will deform homogeneously, but by a different strain from the bulk strain (i.e. far-field strain in the matrix), if there is a viscosity contrast. Experiments (Gay 1968a) and finite-element models (Shimamoto 1975) verify the theory, and indicate that inclusions whose centres are spaced more than twice their diameters apart will not influence each other, so may in practice be considered as isolated.

Much of the work cited above concerns pure shear of isolated elliptical cylinders, which in two dimensions is the deformation of elliptical inclusions. Bilby *et al.* (1975) presented an algebraic solution (slightly different from that of Gay 1968a) for initially circular inclusions in pure shear, which will be rewritten here in the nomenclature used for $R_f/\phi$ analysis (Lisle 1985 and references therein):

$$\ln R_s = \ln R_f + \{(m-1)(R_f - 1)/(R_f + 1)\}. \quad (1)$$

$R_s$ is the bulk strain ratio, $R_f$ is the final inclusion axial ratio, which in this case is the inclusion strain ratio, and $m$

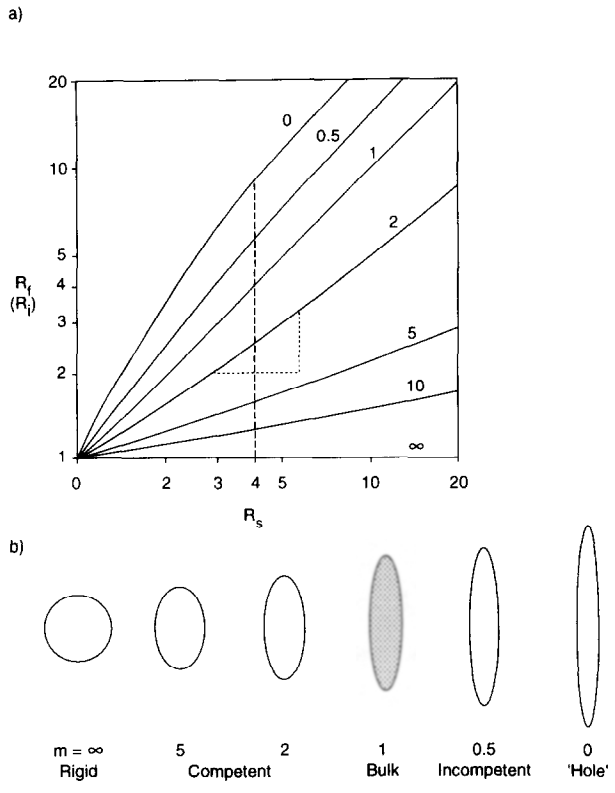


Fig. 1. (a) Graphical represention of equation (1), after Gay (1976), (fig. 1, after Bilby *et al.* 1975). Numbers on the curves give viscosity ratio, $m$. The dashed ordinate line for $R_s = 4$ (50% shortening) provides the data for the ellipses in (b), initially circular, with viscosity ratio numbered, and the bulk strain ellipse shaded.

is the (Newtonian) viscosity ratio (inclusion/matrix). Figure 1(a) represents this equation graphically, and Fig. 1(b) gives final shapes for 50% bulk shortening ($R_s = 4$) and different viscosity ratios. For $m > 10$, inclusion strain will be small, and the inclusion may be considered as nearly rigid ($m = \infty$). At the other extreme, the $m = 0$ curve, representing a fluid-filled hole (Bilby *et al.* 1976), is the maximum possible inclusion deformation: not an infinite strain, as might be expected, but $R_f/R_s < 2.7$ (for $R_s < \infty$). This limiting value provides a useful 'rule-of-thumb' for determining bulk strain from the most incompetent of deformed strain markers.

An explicit expression like equation (1) cannot be written for initially elliptical inclusions, but Lisle (1985, chapter 7) presents sets of $R_f/\phi$ graphs which allow deformed shapes of inclusions of different initial axial ratios, orientations and viscosity ratios to be determined. Alternatively, Fig. 1(a) can be used for initial elliptical inclusions aligned parallel to principal bulk stretch. For example (see dashed triangle, Fig. 1a), an 'initial ellipse' with $R_i = 2$, on the $m = 2$ curve deforms by a bulk strain of $R_s = 2$ (abscissa distance) to the final inclusion axial ratio, $R_f \approx 3.3$. The deformation paths in Fig. 1(a) are only slightly non-linear, so it may be deduced that the original or developing ellipticity has only a slight influence on the *increment* of inclusion deformation.

Gay (1968b), Gay & Fripp (1976) and Lisle *et al.* (1983) apply two-dimensional inclusion theory to naturally deformed rocks, such as conglomerates. All assume that the inclusions were initially circular or elliptical in section. These studies deduced only small viscosity ratios between pebbles and matrix, for various rock and mineral types (less than 10:1), which is lower than is generally inferred from analyses of single-layer folds (e.g. Sherwin & Chapple 1968).

*Rules for ellipsoids and non-ellipsoids*

The theory of deformable inclusions, outlined above, is principally concerned with ellipsoidal inclusions. Eshelby (1957) demonstrated that an isolated ellipsoidal inclusion in material contrast with its matrix deforms in uniform strain, and so an ellipsoidal inclusion shape is maintained. However, he also considered non-ellipsoidal inclusions, and showed that *non-ellipsoidal inclusions deform by inhomogeneous strain.* It follows that the inclusion shape will become irregular. This result has potential importance for geological strain markers. It means that any non-spherical or non-ellipsoidal inclusion (with a viscosity contrast) should not be considered as a homogeneously strained marker, and cannot be represented by a single strain ellipsoid. Such inclusions must change their geometrical form during deformation, so a cube will not deform to a cuboid, and a prismatic inclusion not retain its straight edges. The shape change will be driven by the type of heterogeneous strain, and irregularities will amplify or diminish.

A full examination of the deformation of inclusions of various initial shapes, and for different types of deformation, is the subject of our ongoing research. Before presenting some preliminary modelling, we briefly discuss the possible range of initial shapes of geological inclusions and clasts.

## GEOLOGICAL INCLUSIONS: SHAPES OF CLASTS AND GRAINS

There are many types of geological object that might be considered as inclusions, ranging from volcanic clasts, concretions and fossils to large crystals, grains and pebbles. We concentrate on the latter set, in this study. According to recent analyses of clast shape (e.g. Diepenbroek *et al.* 1992, and references therein), it is generally assumed that the 'ultimate shape' of a *sedimentary particle* subjected to prolonged 'rounding' is an ellipsoid. This ideal seems to apply to all sedimentary clasts, from sand or silt size to pebbles and cobbles. However, Fourier analysis of shapes of 25–50 mm fluvial and coastal clasts from Calabria, Italy (Diepenbroek *et al.* 1992) does not indicate perfect rounding to an ellipsoidal form, despite a crude axial symmetry (axial ratios 1:1:1.36).

Lisle (1988) set out to test the 'ellipsoid assumption' on round beach pebbles from Gower, Wales. He concluded that the 'average pebble' shape was superelliptical in cross-section, and in three dimensions, an oblate 'superellipsoid of revolution'. Following Lisle (1988) (see Fig. 2), the superellipse to subellipse geometry is described in

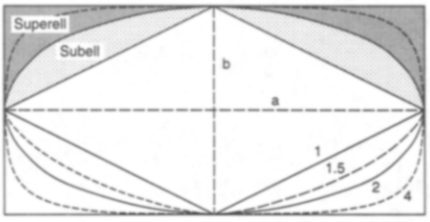


Fig. 2. The description of Lisle (1988) of subellipse to superellipse geometry, described in Cartesian coordinates by $(x/a)^p + (y/b)^p = 1$. $x$ is parallel to the $a$ diameter, $y$ is parallel to the $b$ diameter. Numbers are $p$ values. See text and equation (2).

Cartesian coordinates by:

$$(x/a)^p + (y/b)^p = 1. \quad (2)$$

For $p = 2$, this becomes the equation for an ellipse with axial ratio $a/b$. Subellipses have $p < 2$, and superellipses $p > 2$. Lisle's 'average pebble shape' had $p = 2.6$ and axial ratio 2.7. These data would appear contradictory to the statement by Burns & Spry (1969) that most *deformed* pebbles (in conglomerates) have nearly ellipsoidal shapes. However, our modelling may provide reasons for the apparent contradiction.

The shapes of *porphyroblasts* and *porphyroclasts* deserve mention, because of their use and potential as deformation markers. Porphyroclast structures such as 'tails' and 'wings' are widely used as 'shear criteria' (Simpson and Schmid 1983, Passchier & Simpson 1986, Hanmer & Passchier 1991), and the symmetry used to distinguish coaxial from non-coaxial deformation (Choukroune *et al.* 1987). Feldspar porphyroclasts with $\sigma$ or $\delta$ 'wings' have been modelled as spherical objects with a rigid core and soft outer shell (Passchier & Sokoutis 1993). However, many illustrated examples of mantle-clast structures (e.g. Hanmer & Passchier 1991, figs. 46, 47 and 50) appear to show evidence for clasts far more rectilinear than circular. We suggest that cubic, cuboidal and prismatic shapes may be more appropriate than spheres or ellipsoids, for general modelling of porphyroblasts and porphyroclasts.

A study of the deformation of initially square-sectioned inclusions of different viscosity ratio can therefore serve a dual purpose: (1) to indicate expected deformed shapes for square or rectangular inclusions, such as porphyroclasts; and (2) combined with evidence for ellipses, to indicate deformation of intermediate forms, such as subelliptical and superelliptical inclusions, relevant to sedimentary clasts.

## MODELLING THE DEFORMATION OF SQUARE INCLUSIONS

### *Evidence from boudins*

Boudin shapes provide important data on the deformation of stiff rectilinear geological inclusions. The progressive development of barrel-shaped and eventually fish mouth-shaped boudins has long been described from rocks, and in theory and experiments (Ramberg 1955, Ramsay 1967, p. 106, Strömgård 1973). The experimental results of Ghosh & Ramberg (1976), (figs. 34–41), and the finite-element simulations of Lloyd & Ferguson (1981), indicate that the process of 'corner deformation' occurs also in single inclusions of initial rectangular form. However, the extreme barrelled and hooked form modelled by Lloyd & Ferguson (1981) depended on plastic deformation, and less extreme shapes might be expected for Newtonian models.

What, then, might be expected for a rectilinear inclusion that is less viscous than the matrix? Logically, an 'antibarrel' shape might be anticipated, with an opposite type of corner effect from those seen in competent boudins. Lisle (1973, fig. 71) illustrated this effect schematically, as an 'axe-head' type of shape. We now present some finite-element models to explore these possible shape changes more exactly.

### *Finite-element modelling of square inclusions in pure shear*

A two-dimensional finite-element code that treats the case of plane-strain steady-state flow in incompressible fluids (Lan & Hudleston 1991) is used in this study. The finite-element model consists of a central square inclusion, aligned either with the coordinate frame or diagonally, and a surrounding matrix. Both the inclusion and matrix are treated as Newtonian fluids, with viscosity ratio, $m$. The model is divided into 760–780 triangular and quadrilateral elements. Symmetry of the structure has been used to reduce the number of elements needed for the computations. All models are deformed to 50% shortening (i.e. $R_s = 4$, in equation 1, and Fig. 1).

Figure 3 presents the deformed inclusion shapes, for a range of viscosity ratios. The central shaded rectangle and rhomb are the expected shapes for homogeneous deformation, where there is no viscosity contrast ($m = 1$). In cases with viscosity contrast, there are two concurrent processes causing the shape changes. (1) The overall dimensions of the inclusions change, according to the viscosity contrast, with the least deformation at the highest $m$. The shapes change irregularly, according to the degree of heterogeneous deformation; for example, as seen by 'corner deformations'. There appear to be critical values of $m$, for both competent and incompetent inclusions, where these heterogeneous effects are maximum.

*Competent inclusions* aligned with the coordinate frame (Fig. 3a, $m > 1$) show varying degrees of barrelling and pulled-out corners, as described for some boudins. However, the same competent inclusions, but in diagonal orientation (Fig. 3b), only slightly deviate from rhomb towards lemon shapes. For both orientations, the maximum shape irregularity appears close to $m = 5$.

*Incompetent inclusions* (Fig. 3, $m < 1$) provide some surprising results. It was already noted in the discussion of circular inclusions that there is a theoretical 'upper limit' of deformation for $m \to 0$, only a few factors greater than the bulk deformation. This is also true for the square inclusion models, shown by the narrow range of inclusion lengths between $m = 1$ and $m = 0.01$, for both

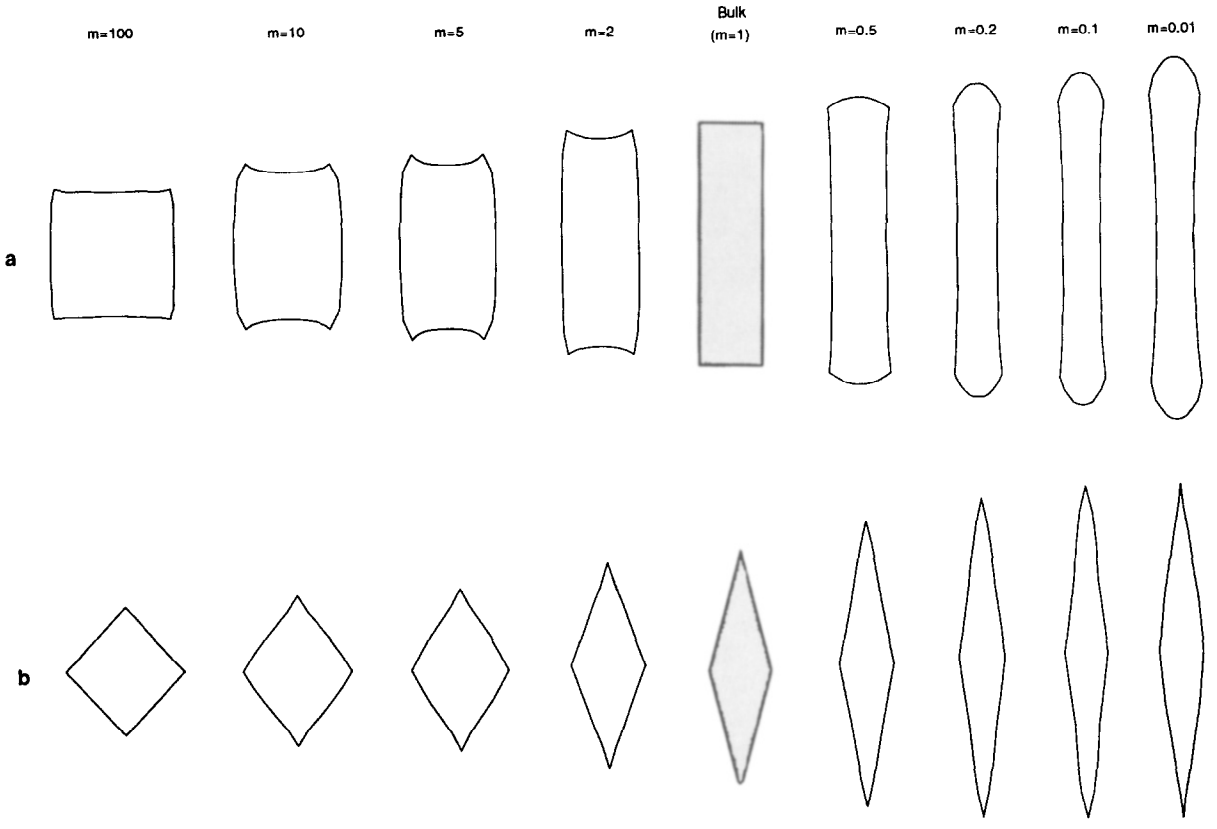


Fig. 3. Finite-element models of 50% pure shear of (a) initially square and (b) diagonal-square inclusions, with inclusion: matrix viscosity ratio ($m$) labelled. The central shaded rectangle and rhomb indicate the bulk deformation, or the shape for $m = 1$. Note the strong shape changes from barrel to bone shapes in (a), compared to smaller variations from rhombs in (b).

orientations. Incompetent inclusions aligned with the coordinate frame (Fig. 3a) show bone to dumb-bell shapes, with a surprisingly large degree of outward bulging at the tips. The most extreme effect, at $m = 0.01$, appears rather like a long double droplet. How many readers, confronted with this this curvaceous shape, would realise that it had once been square? The lobate ends might be particularly surprising, in view of the opposite sense of lobing seen in mullions which develop as a result of mechanical instabilities on planar viscosity boundaries (Ramsay 1967, p. 383, Sokoutis 1987). In comparison with these extreme shape changes, the incompetent diagonal inclusions (Fig. 3b) deform to only slightly irregular sheath-like rhombs, with a maximum shape effect seen at about $m = 0.1$.

These results suggest that a whole variety of shapes could arise from the deformation of initially square inclusions which are asymmetrically oriented with respect to pure shear; or in simple shear. For competent inclusions, we anticipate asymmetric barrel or flag shapes: for incompetent, ribbons or fish shapes.

## DEFORMATION OF INCLUSIONS IN THE CIRCLE TO SQUARE RANGE

By combining the results in Fig. 3 with those for circular inclusions (Fig. 1), we can make some predictions for the deformation of inclusions in the circle to square range, for examples of $m = 5$ and 0.2, and 50% shortening (Fig. 4). Selected shapes for (1) a subellipse and (2) a superellipse are given (Fig. 4, right sides), recalling that the latter have been proposed as a likely shape of sedimentary clasts. For an equant shape, where $a = b$, equation (2) now becomes:

$$x^p + y^p = r^p, \tag{3}$$

with $r$ the initial equant dimension. Our examples in Fig. 4 take $p = 1.5$ for the subellipse or 'subcircle' (curve 1), and $p = 3$ for the superellipse or 'supercircle' (curve 2).

It must first be noted that the deformed lengths on the symmetry axes are different for the circular, rhomb and square inclusions. The difference is slight for the competent inclusions (Fig. 4b), but for the incompetent example (Fig. 4c), the ellipse is measurably longer than the 'bone' and 'rhomb'. We expect the deformed shape for the 'subcircle' (curve 1) to fall in the field between the near-rhomb and the ellipse, and the 'supercircle' (curve 2) to fall between the ellipse and the 'barrel' for $m = 5$, and the ellipse and the 'bone', for $m = 0.2$ (Fig. 4, right). The exact shapes drawn are speculative, but closely controlled by the exact modelling (Fig. 4, left).

This qualitative modelling suggests that a *competent subcircular inclusion* might deform nearly to a subellipse, whereas a *competent supercircle* might become a more irregular 'square ellipse'. For increasing $m$, the effect will

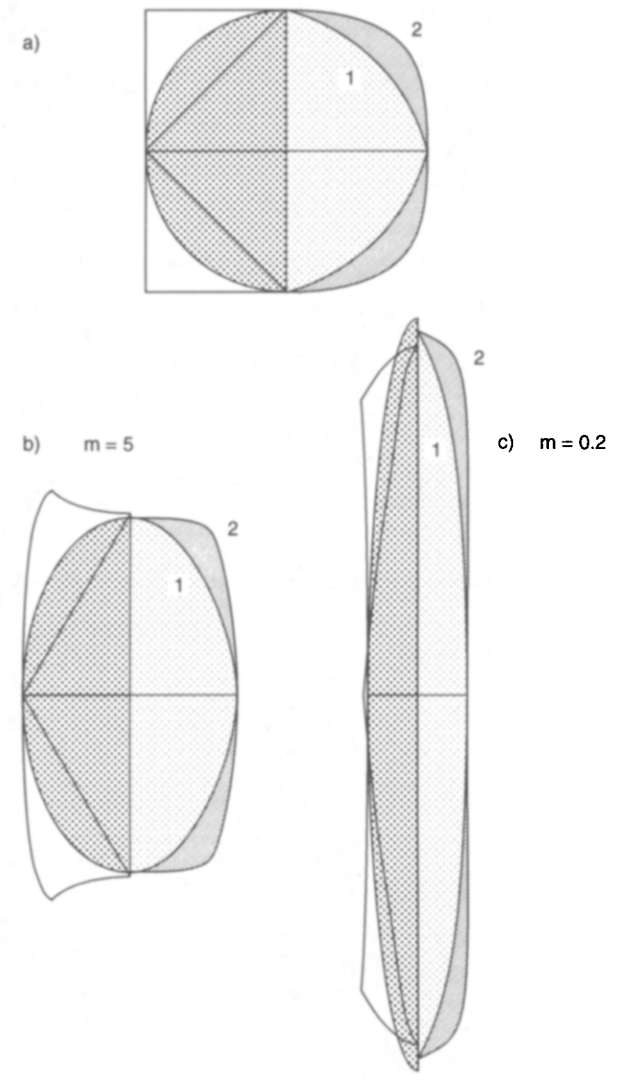


Fig. 4. Compilation with speculations for deformation of inclusions in the circle to square shape range. (a) Initial shapes; (b) $m = 5$; (c) $m = 0.2$. The *left sides* combine information from Figs. 1 and 3, for circles (shaded) and squares (outlines). The *right sides* are examples of (1) a subellipse/subcircle (inner shading), and (2) a superellipse/supercircle (outer shading). See text for discussion.

be less noticeable as the inclusions will be hardly deformed. For *incompetent subcircles*, the deformed shapes may not be significantly different from an extreme *a:b* subellipse, whereas the *incompetent supercircle* will be an almost straight-sided ribbon shape. With sufficient bulk deformation, and given the rounded ends produced even for the initial square shape, *it seems likely that these shapes of incompetent inclusions would be interpreted, by eye, as elongate ellipses.*

## GEOLOGICAL APPLICATIONS

### *Deformed inclusion shapes as a competence criterion*

Distinctly different shapes are produced in our models of deformed square inclusions, according to viscosity ratio and orientation. These initial results suggest that competent inclusions of varied shape will show a lower strain than the matrix, but may increase their shape irregularity. In contrast, incompetent inclusions will deform rather more than the matrix, and we suggest these will become more curved in shape, perhaps indistinguishable from elliptical if deformation is sufficiently strong. Continued work will model strain and shape changes for a wide variety of initial inclusion shapes in progressive deformation, and comparing Newtonian and non-Newtonian rheologies.

### *Implications for clasts, tails and 'fish'*

Tear-drop or lemon-shaped quartz clasts are a common feature of deformed rocks. From the theory and modelling in this paper, any non-elliptical deformed inclusion must *either* have been initially non-elliptical, *or* have resulted from a process which contravened 'isolated inclusion' theory (e.g. interference of adjacent objects, non-isotropic rheology, non-Newtonian flow, etc.). While several of these reasons may be applicable to rocks, where a sigmoidal or tear-drop-shaped clast (e.g. of quartz) is observed in isolation, it might be reasonable to attribute its shape to deformation of an inclusion of originally non-elliptical form. 'Quartz ribbons' in mylonites could provide evidence that the quartz, here, behaved as incompetent inclusions.

Porphyroclast 'tails' and related 'rolling structures' (Passchier & Simpson 1986, Van den Driessche & Brun 1987) are commonly used as sense-of-shear indicators in shear zones. The 'pulling out' of corners in the deformed square inclusions (e.g. Fig. 3, $m = 5$) would appear to provide a mechanisms for initiating wings or tails from rectilinear clasts, as implied in the model of Mawer (1987, fig. 7). Whether a large enough simple shear can produce significant tails and 'rolling structures' in isotropic linear viscous inclusion/matrix systems remains to be tested in further modelling.

*Acknowledgements*—SHT wishes to thank Richard Lisle, John Ramsay, Jack Treagus and Simon Hanmer for lively discussion and comments on possible shape changes of non-ellipsoidal objects, in advance of the FE modelling. Richard Hartley is thanked for drafting the figures. PJH and LL acknowledge support of the National Science Foundation (EAR 9219702) and the University of Minnesota Supercomputer Institute. We appreciate the helpful comments of Chris Talbot.

## REFERENCES

Bilby, B. A., Eshelby, J. D., Kolbuszewski, M. L. & Kundu, A. K. 1976. The change of shape of a viscous ellipsoidal region embedded in a slowly deforming matrix having a different viscosity. Some comments on a discussion by N. C. Gay. *Tectonophysics* **35**, 408–409.

Bilby, B. A., Eshelby, J. D. & Kundu, A. K. 1975. The change of shape of a viscous ellipsoidal region embedded in a slowly deforming matrix having a different viscosity. *Tectonophysics* **28**, 265–274.

Bilby, B. A. & Kolbuszewski, M. L. 1977. The finite deformation of an inhomogeneity in two-dimensional slow viscous incompressible flow. *Proc. R. Soc.* **355**, 335–353.

Burns, K. L. & Spry, A. H. 1969. Analysis of the shape of deformed pebbles. *Tectonophysics* **7**, 177–196.

Choukroune, P., Gapais, D. & Merle, O. 1987. Shear criteria and structural symmetry. *J Struct. Geol.* **9**, 525–530.

Diepenbroek, M., Bartholomä, A. & Ibbeken, H. 1992. How round is round? A new approach to the topic of 'roundness' by Fourier grain shape analysis. *Sedimentology* **39**, 411–422.

Eshelby, J. D. 1957. The determination of the elastic field of an ellipsoidal inclusion, and related problems. *Proc. R Soc.* **241**, 376–396.

Freeman, B. 1987. The behaviour of deformable ellipsoidal particles in three-dimensional slow flows: implications for geological strain analysis. *Tectonophysics* **132**, 297–309.

Gay, N. C. 1968a. Pure shear and simple shear deformation of inhomogeneous viscous fluids. 1. Theory. *Tectonophysics* **5**, 211–234.

Gay, N. C. 1968b. Pure shear and simple shear deformation of inhomogeneous viscous fluids. 2. The determination of the total finite strain in a rock from objects such as deformed pebbles. *Tectonophysics* **5**, 295–302.

Gay, N. C. 1976. The change of shape of a viscous ellipsoidal region embedded in a slowly deforming matrix having a different viscosity—Discussion. *Tectonophysics* **35**, 403–407.

Gay, N. C. & Fripp, R. E. P. 1976. The control of ductility on the deformation of pebbles and conglomerates. *Phil. Trans. R. Soc.* **283**, 109–128.

Ghosh, S. K. & Ramberg, H. 1976. Reorientation of inclusions by combination of pure and simple shear. *Tectonophysics* **34**, 1–70.

Hanmer, S. & Passchier, C. 1991. *Shear Sense Indicators: A Review.* Geological Survey of Canada, Paper 90-17.

Lan, L. & Hudleston, P. J. 1991. Numerical models of buckle folds in non-linear materials. *Tectonophysics* **199**, 1–12.

Lisle, R. J. 1973. The Application of Methods of Structural Analysis to the Study of the Basement Complex of N. W. Lewis. Unpublished Ph. D. thesis, University of London.

Lisle, R. J. 1985. *Geological Strain Analysis. A manual for the $R_f/\phi$ Technique.* Pergamon Press, Oxford.

Lisle, R. J. 1988. The superellipsoidal form of coarse clastic sediment particles. *Math. Geol.* **20**, 879–890.

Lisle, R. J., Rondeel, H. E., Doorn, D., Brugge, J. & van de Gaag, P. 1983. Estimation of viscosity contrast and finite strain from deformed elliptical inclusions. *J. Struct. Geol.* **5**, 603–609.

Lloyd, G. E. & Ferguson, C. C. 1981. Boudinage structure: some new interpretations based on elastic–plastic finite element simulations. *J. Struct. Geol.* **3**, 117–128.

Mawer, C. K. 1987. Shear criteria in the Grenville Province, Ontario, Canada. *J. Struct. Geol.* **9**, 531–539.

Passchier, C. W. & Simpson, C. 1986. Porphyroclast systems as kinematic indicators. *J. Struct. Geol.* **8**, 831–843.

Passchier, C. W. & Sokoutis, D. 1993. Experimental modelling of mantled porphyroclasts. *J. Struct. Geol.* **15**, 895–909.

Ramberg, H. 1955. Natural and experimental boudinage and pinch-and-swell structures. *J. Geol.* **63**, 512–526.

Ramsay, J. G. 1967. *Folding and Fracturing of Rocks.* McGraw Hill, New York.

Sherwin, J.-A. & Chapple, W. M. 1968. Wavelengths of single-layer folds: a comparison between theory and observation. *Am. J. Sci.* **266**, 167–179.

Shimamoto, T. 1975. The finite element analysis of the deformation of a viscous spherical body embedded in a viscous medium. *J. geol. Soc. Japan* **81**, 255–267.

Simpson, C. & Schmid, S. M. 1983. Evolution of criteria to deduce the sense of movement in sheared rocks. *Bull. geol. Soc. Am.* **94**, 1281–1288.

Sokoutis, D. 1987. Finite strain effects in experimental mullions. *J. Struct. Geol.* **9**, 233–242.

Strömgård, K. E. 1973. Stress distribution during formation of boudinage and pressure shadows. *Tectonophysics* **16**, 215–248.

Van den Driessche, J. & Brun, J.-P. 1987. Rolling structures at large shear strain. *J. Struct. Geol.* **9**, 691–704.